



Fermi surface and electronic homogeneity of the overdoped cuprate superconductor $\text{Ti}_2\text{Ba}_2\text{CuO}_{6+\delta}$ as revealed by quantum oscillations

A. F. Bangura,¹ P. M. C. Rourke,¹ T. M. Benseman,² M. Matusiak,² J. R. Cooper,² N. E. Hussey,¹ and A. Carrington¹

¹*H. H. Wills Physics Laboratory, University of Bristol, Tyndall Avenue, Bristol BS8 1TL, United Kingdom*

²*Physics Department, Cavendish Laboratory, University of Cambridge, J. J. Thomson Avenue, Cambridge CB3 0HE, United Kingdom*

(Received 13 September 2010; published 1 October 2010)

We report a quantum oscillation study of $\text{Ti}_2\text{Ba}_2\text{CuO}_{6+\delta}$ for two different doping levels ($T_c=10$ and 26 K) and determine the Fermi-surface size and topology in considerable detail. Our results show that Fermi-liquid behavior is not confined to the edge of the superconducting dome and is robust up to at least $0.3T_c^{\text{max}}$. Superconductivity is found to survive up to a larger doping $p_c=0.31$ than in $\text{La}_{2-x}\text{Sr}_x\text{CuO}_4$. Our data imply that electronic inhomogeneity does not play a significant role in the loss of superconductivity and superfluid density in overdoped cuprates, and point toward a purely magnetic or electronic pairing mechanism.

DOI: [10.1103/PhysRevB.82.140501](https://doi.org/10.1103/PhysRevB.82.140501)

PACS number(s): 74.25.Jb, 74.25.Ha, 74.62.Dh, 74.72.-h

The evolution of the electronic structure with carrier concentration is crucial for understanding the origin of high-temperature superconductivity. In the well-studied hole-doped cuprate $\text{La}_{2-x}\text{Sr}_x\text{CuO}_4$ (LSCO), antiferromagnetism is suppressed beyond $x=0.02$ and superconductivity emerges at $x=0.05$. The superconducting (SC) transition temperature $T_c(x)$ is approximately an inverted parabola maximizing at $x\sim 0.16$ before vanishing at $x=0.27$.¹ Over much of this phase diagram the physical properties are substantially different from those of conventional metals and the range of validity of a Fermi-liquid picture, where the quasiparticles are coherent on all parts of the Fermi surface (FS), is unclear. Although Fermi-liquid behavior may be suggested by transport power laws or the strength of coherence peaks in photoemission experiments, the observation of quantum oscillations (QO) provides unambiguous evidence of quasiparticle coherence at all k points traversed by the electron orbit.²

In fully oxygenated LSCO, it is usually assumed that x equals p , the number of added holes/ CuO_2 unit. Tallon *et al.*³ have argued that T_c follows a universal dependence on p for *all* hole-doped cuprate families, $T_c/T_c^{\text{max}}=1-82.6(p-0.16)^2$. In many families, however, the precise doping level is difficult to determine. Moreover, it has been suggested that hole doping in cuprates is intrinsically inhomogeneous on a length scale of a few unit cells.⁴⁻⁷ NMR experiments on $\text{YBa}_2\text{Cu}_3\text{O}_{7-\delta}$, however, suggest that (static) phase separation is *not* a generic property of underdoped or optimally doped cuprates.⁸ This is supported by analysis of heat-capacity data for $\text{Bi}_2\text{Sr}_2\text{CaCu}_2\text{O}_{8+\delta}$ over a wide range of p , and of NMR data for $\text{YBa}_2\text{Cu}_4\text{O}_8$ and Ca-doped $\text{YBa}_2\text{Cu}_3\text{O}_{7-\delta}$.⁹ For overdoped (OD) cuprates, the applicability of the phase-separation picture is still debated. Experimentally, the ratio of the superfluid density n_s to the carrier effective mass m^* is found to decrease with increasing p .^{10,11} This so-called “boomerang” effect has been attributed either to pair breaking in an inhomogeneous electronic state,¹⁰ or to spontaneous phase separation into hole-rich (non-SC) and hole-poor (SC) regions.^{5,11-13}

Here, we report a detailed study of the de Haas-van Alphen (dHvA) effect in $\text{Ti}_2\text{Ba}_2\text{CuO}_{6+\delta}$ (Ti2201) single crystals with two different T_c values. Our results show that a Fermi-liquid picture extends into the high- T_c phase of OD cuprates

and is not confined to the edge of the SC dome. We show that OD Ti2201 has a highly homogenous electronic state on a length scale of ~ 1000 Å. Our precise determination of the FS volume reveals that superconductivity in Ti2201 survives up to $p_c=0.31$, significantly beyond that inferred for LSCO. The lack of nanoscale inhomogeneity implies that the rapid loss of superfluid density with overdoping is likely due to pair breaking driven by a weakening of the pairing interaction. Finally, the dHvA mass does not change much with p and seems to correspond to an overall band narrowing rather than strong renormalization near the Fermi level. These two facts tend to rule out pairing mechanisms involving low-frequency bosons for these overdoped cuprates.

Ti2201 crystals were grown using a self-flux method¹⁴ and annealed in flowing oxygen at various temperatures to achieve a range of T_c values.¹⁴ Torque magnetization was measured using a piezoresistive microcantilever in a ³He cryostat in the 45 T hybrid magnet in Tallahassee. The tetragonal crystal structure and orientation were determined by x-ray diffraction.

In the inset of Fig. 1 we show torque data for samples with two different doping values ($T_c=10$ and 26 K) after subtracting a third-order polynomial fit to raw data obtained

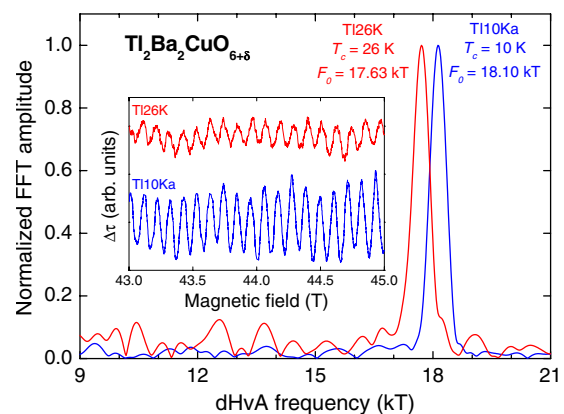


FIG. 1. (Color online) Fast Fourier transform of torque data between 38 and 45 T for Ti26K (red) and Ti10Ka (blue) samples. The data were taken at $T=0.35$ K. The inset shows the raw data for the two samples.

at $T=0.4$ K. (Hereafter, crystals are identified by their T_c values prefixed by the letters “TI”.) Clear dHvA oscillations are seen in both cases. As shown in the main panel, fast Fourier transforms (FFTs) of the raw data show a single sharp peak in the spectra. Note that the slow period oscillations which are evident in the raw data are not intrinsic. The clear shift of the dHvA frequency F to a lower value for the higher T_c sample confirms that the oscillations do not arise from any part of the sample which is not superconducting. Although experiments were made on a large number of samples with different T_c (up to 60 K) in fields up to 70 T (in Toulouse), clear oscillations were only seen on three crystals and weak signals in one other. Samples with low impurity scattering, high crystallographic quality, and high doping homogeneity are needed to observe dHvA oscillations arising from such large FS sheets. For example, a factor 2 decrease in the impurity mean-free-path ℓ_0 from the present values would result in a reduction in the dHvA amplitude of 10^5 , burying the signal firmly into the noise.

Fitting the angle dependence $F(\theta)$ to the expression for a two-dimensional (2D) FS ($=F_0/\cos\theta$), we obtain a fundamental frequency F_0 of 18.10(3) kT and 18.00(1) kT for T110Ka and T110Kb, respectively, in agreement with a previous study in pulsed fields,^{2,15} and 17.63(1) kT for T126K. Note that the width of the FFT peak in Fig. 1 is determined by the field range and is not a measure of the accuracy in $F(\theta)$. F_0 gives directly the extremal cross-sectional area \mathcal{A} of the FS via the Onsager relation $\mathcal{A}=2\pi eF_0/\hbar$. As \mathcal{A} does not vary appreciably with k_z (see later) we can determine the carrier concentration $(1+p)$ via Luttinger’s theorem, $1+p=2\mathcal{A}/(2\pi/a)^2$ (where $a=3.86$ Å is the in-plane lattice parameter). From the frequencies, we obtain hole dopings, p , of 0.304(2), 0.297(1), and 0.270(1), respectively for T110Ka, T110Kb, and T126K. These values are consistent with the measured zero-temperature Hall number $n_H(0)=1.28(6)/Cu$ for a $T_c=15$ K sample.¹⁶

We determine the quasiparticle effective mass by analyzing the T dependence of the dHvA amplitude A using standard Lifshitz-Kosevich (LK) theory.¹⁷ Results are shown for the three different crystals in Fig. 2. $A(T)$ is well fitted by the standard LK formula showing that possible deviations from the usual thermal population factor (the Fermi function) arising from (marginal) non-Fermi-liquid effects¹⁸ are not apparent for temperatures above ~ 350 mK. From the fits, we obtain effective masses m^* of $5.8(3)m_e$, $4.9(3)m_e$, and $5.0(3)m_e$ at $\theta=0^\circ$ for T110Ka, T110Kb, and T126K, respectively. To check for consistency and any field dependence of the dHvA mass (which is common in heavy fermion systems) we compare these values to the zero-field electronic specific heat. For a 2D metal, the Sommerfeld coefficient $\gamma=(\pi k_B^2 N_A a^2/3\hbar^2)m^*$ (where k_B is the Boltzmann constant and N_A Avogadro’s constant).¹⁹ Taking the average $m^*=5.2(4)m_e$ we obtain $\gamma=7.6(6)$ mJ mol⁻¹ K⁻² in excellent agreement with the almost p -independent value of 7(1) mJ mol⁻¹ K⁻² found from direct measurement of polycrystalline Tl2201.²⁰

Comparison with the band mass $m_b\sim 1.7m_e$, given by density-functional theory band calculations^{21,22} (with the FS area adjusted using the virtual-crystal approximation to match the present doping), reveals a significant enhancement

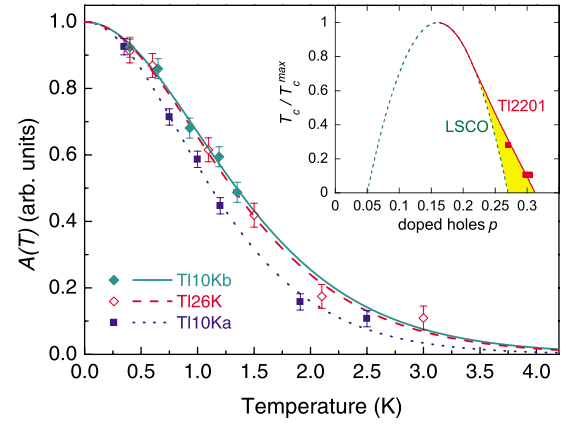


FIG. 2. (Color online) Temperature dependence of the oscillatory torque amplitudes for the three crystals used in this study, fitted to $R_T=\chi/\sinh(\chi)$ with $\chi=14.695m^*T/B\cos\theta$. Field ranges are 40–45 T for T110Ka (squares), 42–45 T for T110Kb (filled diamonds), and 43–45 T for T126K (open diamonds). The inset shows the superconducting T_c versus p dome for LSCO (dashed line) (Ref. 3) and Tl2201 (solid line and squares). The (yellow) shaded area represents the proposed region of suppressed superconductivity in OD LSCO.

due to interaction effects ($m^*/m_b\approx 3$) that is constant (within our uncertainty) up to at least $\sim 0.3T_c^{\max}$. This renormalization is $\sim 20\%$ less than the bandwidth renormalization (which corresponds to $m^*/m_e\sim 6.6$) found by angle-resolved photoemission spectroscopy (ARPES) for OD Tl2201 ($T_c=30$ K).²³ This implies that the renormalization predominantly arises from correlation-induced band narrowing and that any further renormalization close to the Fermi level E_F from interaction with low-energy boson modes is minimal.

Details of the FS topology and spin susceptibility can be determined by measuring the dependence of the dHvA frequency and amplitude on the magnetic field angle with respect to the c axis (θ) and the Cu-O bond direction (φ). Figure 3 shows the FFT amplitudes extracted from field sweeps at $T=0.45$ K for T110Ka (at $\varphi\sim 0^\circ$ and field range

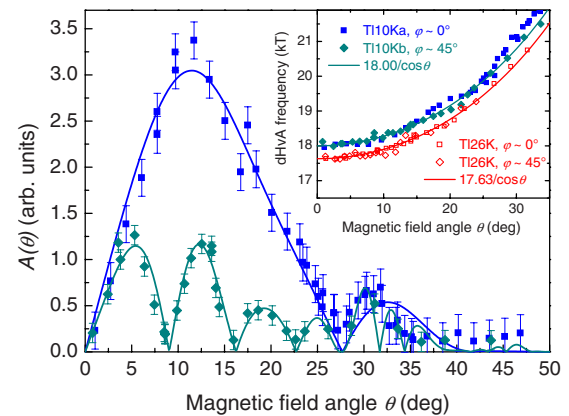


FIG. 3. (Color online) Polar angle dependence of the oscillatory torque amplitude for T110Ka at $\varphi\sim 0^\circ$ (squares) and T110Kb at $\varphi\sim 45^\circ$ (diamonds). The solid line fits to $A(\theta)$ are explained in the text (Ref. 28). The inset shows the polar angle dependence of the dHvA frequencies for all three samples.

42–44 T) and Tl10Kb (at $\varphi \sim 45^\circ$ and field range 42–45 T). Qualitatively similar behavior was observed for the 26 K sample.²¹ For $\varphi \sim 0^\circ$, a broad peak is observed, followed by a minimum that occurs at $\theta \sim 27.5^\circ$. For $\varphi \sim 45^\circ$, the behavior is strikingly different with several clear minima below this angle.

In a quasi-2D metal, minima in $A(\theta, \varphi)$ can be caused by beats between FS sections with nearly equal areas. Following Bergemann *et al.*,²⁴ we expand the FS using cylindrical harmonics compatible with the body-centered tetragonal crystal symmetry

$$k_F(\varphi, \kappa_z) = \sum_{m,n} k_{mn} \cos(n\kappa_z) \times \begin{cases} \cos(m\varphi) (m=0, 4, 8, \dots) \\ \sin(m\varphi) (m=2, 6, 10, \dots) \end{cases}. \quad (1)$$

As the FS is close to 2D we determined the dHvA frequencies and amplitudes from FFTs of the oscillatory magnetization calculated using the full superposition integral, $M \propto \int_0^\pi dk_z \sin(\hbar A(k_z)/eB)$ [where $A(k_z)$ is determined from numerical integration of $k_F(\varphi, \kappa_z)$ including spin splitting] rather than the more usual extremal approximation.²⁴ As a guide we use the same components (k_{00} , k_{40} , k_{21} , k_{61} , and k_{101}) that were used to map out the FS topology of OD Tl2201 by angle-dependent magnetoresistance (ADMR).^{25,26} The FS volume (and hence $1+p$) is determined by k_{00} alone and this is precisely determined by the mean dHvA frequency. For $\varphi=0$, the $n=1$ warpings do not give rise to beats for any θ and hence at low θ , where spin-splitting effects are negligible, data for the field dependence of the amplitude for this direction can be simply related to dHvA phase-smearing effects as discussed further below.

For $\varphi \sim 45^\circ$, the minima observed below $\theta=25^\circ$ are determined by k_{21} , the dominant component of the c -axis warping, which is a parameter that cannot be determined directly by ADMR or ARPES. Our data show that $k_{21} = -1.70(5) \times 10^7 \text{ m}^{-1}$ and $-1.25(5) \times 10^7 \text{ m}^{-1}$ for $T_c=10 \text{ K}$ and 26 K , respectively, corresponding to a resistivity anisotropy ρ_c/ρ_{ab} of $3.3(2) \times 10^3$ and $6.2(5) \times 10^3$ (assuming isotropic scattering) and a significant increase in the electrical anisotropy as T_c^{max} is approached. Experimentally $\rho_c/\rho_{ab} \approx 2.5 \times 10^3$ at low temperature for samples with $T_c \leq 25 \text{ K}$.²⁷

Minima in $A(\theta, \varphi)$ can also occur due to spin splitting, and a “spin zero” is expected when the spin-up and spin-down FS areas differ by a half-integral number of Landau quanta.¹⁷ The location of these “spin zeros” is determined by the spin mass m_{sus} , which is generally not the same as m^* .²⁴ As no minima due to FS warping are expected for $\varphi=0$ we attribute the minimum that occurs at $\theta \sim 27.5^\circ$ to such spin splitting. Because only one minimum is observed, m_{sus} is not strongly constrained but 27.5° is consistent with a number of m_{sus}/m_e values (e.g., 3.99, 4.87, and 5.76), which are all close to the measured thermodynamic mass m^* .

The suppression of the dHvA amplitude with field and angle is controlled by a combination of impurity scattering, doping inhomogeneity, and mosaic spread. It is difficult to disentangle the three effects as they all have similar B dependence over the limited field range where the oscillations are observable. However, by assuming that

each term alone is responsible for the damping we can set upper limits on their individual magnitudes. The Dingle damping term due to impurity scattering is given by $R_D = \exp[-\sqrt{2}\pi^2\hbar F_0/e/(\ell_0 B \cos \theta)]$ while the damping term due to doping inhomogeneity or mosaic spread is $R_p = \exp[-(\pi\alpha/B \cos \theta)^2]$ (where $\alpha = \pi\hbar\delta p/ea^2$ or $F_0 \tan \theta\delta\theta$, respectively—here we have assumed a Gaussian distribution for both).¹⁷ If we ascribe the damping purely to impurity scattering it would correspond to mean-free paths ℓ_0 of $410(10) \text{ \AA}$ for sample Tl10Ka and $360(30) \text{ \AA}$ for Tl26K. Alternatively, if the damping is ascribed to doping inhomogeneity then $\delta p \leq 0.0022(2)$ for all samples. Indeed, were $\delta p > 0.005$, all dHvA phenomena would be so strongly damped as to be rendered unobservable within our current experimental noise floor. This is an important result as it demonstrates that on the length scale of the cyclotron radius r_c at which the quantum oscillations become observable ($r_c = 1200 \text{ \AA}$ at $B=40 \text{ T}$) there are no *intrinsic* processes which cause appreciable “phase smearing” of the dHvA signal in the doping range we have measured. This includes doping inhomogeneity, impurity scattering, and other processes such as a k -dependent pseudogap.

Typical fits for Tl10Ka and Tl10Kb, using $\delta p=0.0025$ (Tl10Ka) and 0.0021 (Tl10Kb), $\delta\theta=0$, and $\ell_0=\infty$, are shown as solid lines in Fig. 3. The overall θ dependence of the amplitude is difficult to model precisely as it depends on knowledge of the mosaic distribution in the crystal as well as the θ, φ dependence of the scattering rate. In particular, we observed a strong asymmetry in the angular dependence for $\varphi \sim 0^\circ$ that is not understood. This asymmetry is much weaker for $\varphi \sim 45^\circ$ and importantly, the positions of the minima, which determine k_{21} , are symmetric with respect to $\pm\theta$.

Collectively, these findings appear to rule out the notion that coexisting hole-rich and hole-poor regions (of order the coherence length) are responsible for the decrease in n_s in OD Tl2201.^{5,11} In the alternative, pair-breaking scenario, the rapid loss of superfluid density is attributed to a crossover from weak to strong pair breaking with overdoping.¹⁰ According to our dHvA data, ℓ_0 is relatively insensitive to carrier concentration, and recent high-field transport measurements on LSCO indicate that the residual in-plane resistivity $\rho_{ab}(0)$ is roughly constant across the entire OD region of the phase diagram.²⁹ Thus for the crossover from clean to dirty limit superconductivity to be realized, overdoping must be accompanied by a marked reduction in the strength of the pairing interaction,^{10,30} as implied by the observed correlation between T_c and the magnitude of the (anisotropic) T -linear scattering rate in OD LSCO (Ref. 29) and Tl2201.³¹

The SC phase diagram of OD Tl2201 is compared with that of LSCO in the inset to Fig. 2. The dashed line is the “universal” parabola,³ scaled to T_c^{max} , while the solid line is the corresponding $T_c(p)$ curve for Tl2201, as determined by this study (black squares). (Here we have assumed that T_c^{max} remains at $p=0.16$.) Extrapolation of the solid line in Fig. 2 to $T_c=0$ implies that superconductivity in Tl2201 will disappear at $p=0.31$. In LSCO, the T -linear term in ρ_{ab} persists to $x=0.29$, i.e., outside the LSCO SC dome,²⁹ implying that pairing may still be active there. Indeed, comparison of the impurity scattering rate with Δ_0 suggests that the parabolic

tail off of $T_c(p)$ in LSCO could be caused by the same pair-breaking effects that lead to the reduction in n_s/m^* . In LSCO ($x=0.29$), $\rho_{ab}(0) \sim 18 \mu\Omega \text{ cm}$.²⁹ Taking FS parameters for OD LSCO from ARPES,³² we obtain a transport (i.e., large angle) scattering rate $\hbar/\tau_0 \sim 10 \text{ meV}$ that is much larger than the BCS weak-coupling value $\Delta_0 = 2.14k_B T_c \sim 2 \text{ meV}$, for $T_c \approx 10 \text{ K}$. In contrast, for Tl2201 with $T_c = 10 \text{ K}$, $\rho_{ab}(0) \sim 6 \mu\Omega \text{ cm}$ (Ref. 33) and correspondingly, $\hbar/\tau_0 \sim 3 \text{ meV} \approx \Delta_0$.

In conclusion, detailed angle-dependent QO experiments indicate that there is no phase separation in OD Tl2201 over a length scale of hundreds of angstroms. All indicators suggest that the physical properties of OD Tl2201 are determined by a single, spatially homogeneous Fermi-liquid electronic state that is now very well characterized. We therefore conclude that pair breaking (possibly enhanced by the effect of a pairing interaction that is highly anisotropic) is responsible for the loss of superfluid density in OD Tl2201 and probably for the disappearance of super-

conductivity in LSCO below $p_c = 0.31$. The underlying reason for this appears to be the rapid fall in the strength of the pairing interaction on the OD side.^{10,30} This, and the absence of any significant renormalization near the Fermi level support a purely magnetic or electronic mechanism. Our findings also provide further experimental evidence that superconductivity persists to much higher doping levels than the normal-state pseudogap. We stress here that the closure of the pseudogap is not field induced since the FS parameters found here are entirely consistent with zero-field transport,¹⁶ thermodynamic²⁰ and spectroscopic²³ data.

We thank L. Balicas, A. I. Coldea, C. Proust, D. Vignolles, B. Vignolle, I. Kokanović, A. P. Mackenzie, D. A. Bonn, W. N. Hardy, R. Liang, and B. J. Ramshaw for their contributions to this project. This work was supported by the EPSRC (U.K.), the Royal Society and a cooperative agreement between the State of Florida and NSF.

- ¹H. Takagi, T. Ido, S. Ishibashi, M. Uota, S. Uchida, and Y. Tokura, *Phys. Rev. B* **40**, 2254 (1989).
- ²B. Vignolle *et al.*, *Nature (London)* **455**, 952 (2008).
- ³J. L. Tallon, C. Bernhard, H. Shaked, R. L. Hitterman, and J. D. Jorgensen, *Phys. Rev. B* **51**, 12911 (1995).
- ⁴V. J. Emery and S. A. Kivelson, *Physica (Amsterdam)* **209C**, 597 (1993).
- ⁵Y. J. Uemura, *Solid State Commun.* **120**, 347 (2001).
- ⁶S. H. Pan *et al.*, *Nature (London)* **413**, 282 (2001).
- ⁷K. McElroy *et al.*, *Science* **309**, 1048 (2005).
- ⁸J. Bobroff, H. Alloul, S. Ouazi, P. Mendels, A. Mahajan, N. Blanchard, G. Collin, V. Guillen, and J.-F. Marucco, *Phys. Rev. Lett.* **89**, 157002 (2002).
- ⁹J. W. Loram, J. L. Tallon, and W. Y. Liang, *Phys. Rev. B* **69**, 060502(R) (2004).
- ¹⁰Ch. Niedermayer, C. Bernhard, U. Binniger, H. Glückler, J. L. Tallon, E. J. Ansaldo, and J. I. Budnick, *Phys. Rev. Lett.* **71**, 1764 (1993).
- ¹¹Y. J. Uemura *et al.*, *Nature (London)* **364**, 605 (1993).
- ¹²Y. Tanabe *et al.*, *J. Phys. Soc. Jpn.* **74**, 2893 (2005).
- ¹³Y. Wang, J. Yan, L. Shan, H.-H. Wen, Y. Tanabe, T. Adachi, and Y. Koike, *Phys. Rev. B* **76**, 064512 (2007).
- ¹⁴A. W. Tyler, Ph.D. thesis, Cambridge University, 1997.
- ¹⁵The difference in F_0 between the two 10 K samples could be due to a small $\sim 5^\circ$ misalignment of the sample along the axis perpendicular to the rotation axis.
- ¹⁶A. P. Mackenzie, S. R. Julian, D. C. Sinclair, and C. T. Lin, *Phys. Rev. B* **53**, 5848 (1996).
- ¹⁷D. Shoenberg, *Magnetic Oscillations in Metals* (Cambridge University Press, Cambridge, 1984).
- ¹⁸A. Wasserman *et al.*, *J. Phys.: Condens. Matter* **3**, 5335 (1991).
- ¹⁹A. P. Mackenzie *et al.*, *Physica (Amsterdam)* **263C**, 510 (1996).
- ²⁰J. M. Wade *et al.*, *J. Supercond.* **7**, 261 (1994).
- ²¹P. M. C. Rourke, A. F. Bangura, T. M. Benseman, M. Matusiak, J. R. Cooper, A. Carrington, and N. E. Hussey, *New J. Phys.* (to be published).
- ²²S. Sahrakorpi *et al.*, *Physica (Amsterdam)* **C460-C462**, 428 (2007).
- ²³M. Platé *et al.*, *Phys. Rev. Lett.* **95**, 077001 (2005).
- ²⁴C. Bergemann *et al.*, *Adv. Phys.* **52**, 639 (2003).
- ²⁵N. E. Hussey *et al.*, *Nature (London)* **425**, 814 (2003).
- ²⁶The parameters k_{40} , k_{61} , and k_{101} are not well determined by our dHvA measurements and are fixed at the values determined by ADMR (Ref. 31), e.g., for $T_c = 10 \text{ K}$ we used $k_{40}/k_{00} = -0.0315$, $k_{61}/k_{21} = 0.71$, and $k_{101}/k_{21} = -0.25$.
- ²⁷N. E. Hussey, J. R. Cooper, J. M. Wheatley, I. R. Fisher, A. Carrington, A. P. Mackenzie, C. T. Lin, and O. Milat, *Phys. Rev. Lett.* **76**, 122 (1996).
- ²⁸Azimuthal angles of $\varphi = 6^\circ$ and 45° were assumed for the fits.
- ²⁹R. A. Cooper *et al.*, *Science* **323**, 603 (2009).
- ³⁰J. G. Storey, J. L. Tallon, and G. V. M. Williams, *Phys. Rev. B* **76**, 174522 (2007).
- ³¹M. Abdel-Jawad, J. G. Analytis, L. Balicas, A. Carrington, J. P. H. Charmant, M. M. J. French, and N. E. Hussey, *Phys. Rev. Lett.* **99**, 107002 (2007).
- ³²T. Yoshida *et al.*, *J. Phys.: Condens. Matter* **19**, 125209 (2007).
- ³³C. Proust, E. Boaknin, R. W. Hill, L. Taillefer, and A. P. Mackenzie, *Phys. Rev. Lett.* **89**, 147003 (2002).